Nonlinear Dynamics and Systems Theory, **25** (4) (2025) 457–470

Exploring Boundary Layer Flow Dynamics on a Semi-Infinite Plate: A Numerical Study of Transpiration Effects and Dual Solutions

Mahmmoud M. Syam [1], Rahmah Al-Qatbi [2], Mays Haddadi [2], Alreem Alameri [2] and Muhammed I. Syam [2*]

[1] *Mechanical and Industrial Engineering Department, Abu Dhabi University, P.O.Box 59911, Abu Dhabi, UAE.*
[2] *Department of Mathematical Sciences, UAE University, Al-Ain, United Arab Emirates.*

Received: September 24, 2024; Revised: Jully 22, 2025

Abstract: This paper explores the flow of a uniform stream with no pressure gradient on a parallel semi-infinite plate. This study unveils a novel perspective on the significant influence of the mass transfer parameter and the velocity parameter on the behavior of self-similar boundary layer flows over moving surfaces, governed by the Prandtl boundary layer equations. The analysis reveals that these parameters are pivotal in determining the existence and multiplicity of solutions, which may include no solution, a unique solution, or dual solutions, depending on their specific values. The modified operational matrix method was employed to reduce the complex nonlinear system to a manageable linear third-order boundary value problem, facilitating a more thorough investigation. The numerical validations conducted, including the calculation of L_2-truncation errors, comparison with exact boundary conditions, and consistency checks against established results in the literature, not only affirm the robustness and accuracy of the proposed method but also instill confidence in its reliability. This work contributes to understanding boundary layer flows over moving surfaces by elucidating the critical roles of mass transfer and velocity parameters. It offers a reliable numerical method for solving these complex fluid dynamics problems and provides valuable insights into the physical phenomena governing such flows.

Keywords: *Prandtl boundary layer equations; heat and mass transfer, boundary layer; dual solutions; semi-infinite plate.*

Mathematics Subject Classification (2020): 93C20, 93A30, 93C95.

* Corresponding author: mailto:m.syam@uaeu.ac.ae

1 Introduction

Different studies over the past few decades have demonstrated the presence of multiple solutions in boundary layer flows driven by moving surfaces, both with and without external pressure gradients. This paper presents a novel examination of the uniform flow over a belt moving towards or away from the origin at a constant speed. This topic is closely related to the seminal works by Klemp and Acrivos [1] and Syam [2], who explored the flow induced by finite and semi-infinite flat plates moving at a constant velocity beneath a uniform mainstream. In the scenario where a similarity reduction to an ordinary differential equation is applicable, dual solutions were identified when the plate moved toward the oncoming stream. Mourad et al. [4] and others [5, 6] investigate the multiple solutions to the Falkner–Skan equation in the flow over a stretching boundary. The authors explore the conditions under which dual solutions emerge, specifically focusing on how variations in boundary stretching influence the flow characteristics. They provide a detailed mathematical analysis, demonstrating that the Falkner–Skan equation admits more than one solution under specific parameter regimes. This work contributes to understanding boundary layer behavior in fluid dynamics, particularly in cases where stretching boundaries are present. Hussaini et al. [3] and others [7, 8] later confirmed the non-uniqueness of the similarity solutions for a boundary layer problem involving an upstream-moving wall. The study analyzes the impact of the wall's motion on the boundary layer flow, identifying conditions that lead to multiple solutions. Through a rigorous mathematical approach, the authors demonstrate the existence of non-unique similarity solutions and give a deep understanding of the behavior of the boundary layer under these conditions. Their findings highlight the complexities of upstream-moving walls in fluid dynamics and contribute to a deeper understanding of boundary layer theory. As part of a broader investigation of the Falkner–Skan flows with stretching boundaries, these novel findings open up new avenues for research in the field of fluid dynamics and boundary layer flows. A mathematically analogous problem on the uniform viscous flow over a moving plate arises in the mixed convection boundary layer flow within a fluid-saturated porous medium adjacent to a heated vertical semi-infinite rigid plate. The governing similarity equations include a nondimensional parameter that quantifies the balance between natural and forced convection with two primary scenarios. In the first scenario, where buoyancy and the uniform external flow are aligned, the solutions are singular, as discussed by Cheng [5]. In the second scenario, where buoyancy opposes the uniform external flow, in [9–12], the authors identified the exact dual solutions mentioned in [1–8], where the investigation of the mixed convection boundary layer flow along a vertical surface within saturated porous medium yields significant findings. The study examines the combined effects of natural and forced convection on the boundary layer, offering a detailed analysis of the governing equations. Merkin identifies the critical parameters that influence the flow behavior and provides solutions that describe the boundary layer's response to varying conditions. This work enhances the understanding of convection processes in porous media, particularly in vertical configurations, and underscores the complex interactions between buoyancy-driven and externally imposed flows. Of particular relevance to this study are Merkin and some subsequent works [13–15], which explore the phenomenon of dual solutions in mixed convection within a porous medium. The studies delve into the conditions under which multiple solutions arise, mainly focusing on the interplay between natural and forced convection. The authors present a comprehensive analysis, showing that dual solutions can occur depending on the relative strength of

buoyancy forces compared to the imposed flow. Finally, Weidman et al. [20] and other authors [17–19] present a unified formulation for stagnation-point flow overstretching surfaces, introducing new findings in this area of fluid dynamics. The authors develop a comprehensive and exhaustive mathematical model that encapsulates various cases of stagnation-point flow, incorporating both classical and stretching boundary conditions. Through their analysis, they uncover novel results that extend the understanding of how stretching surfaces influence flow behavior near stagnation points. This work contributes significantly to the field, offering insights and generalizations that enhance the theoretical framework for studying stagnation-point flows. This work, with its thorough and comprehensive nature, provides significant insights into the complexities of mixed convection in porous media and contributes to a broader understanding of fluid behavior in such environments. These implications are crucial for further research and applications in the field of fluid dynamics and boundary layer flows.

2 Mathematical Model

When a uniform stream with velocity U flows parallel to a semi-infinite plate positioned at $y = 0$ for $x \geq 0$, the flow exhibits no pressure gradient. The velocity components in the directions along and perpendicular to the plate are denoted as u and v, respectively. The dimensional unsteady Prandtl boundary layer equations governing this scenario are

$$\frac{\partial u}{\partial x} = -\frac{\partial v}{\partial y}, \tag{1}$$

$$\frac{\partial u}{\partial t} + u\frac{\partial u}{\partial x} = \eta\frac{\partial^2 u}{\partial y^2} - v\frac{\partial u}{\partial y} \tag{2}$$

with boundary conditions specified as

$$u(x,0) = \alpha_2 U, \quad v(x,0) = -\alpha_1\sqrt{\frac{\eta U}{2x}}, \quad x > 0, \tag{3}$$

$$u = U, \quad x \in \mathbb{R}, \quad y \to \infty. \tag{4}$$

Figure 1 illustrates the physical setup of the model.

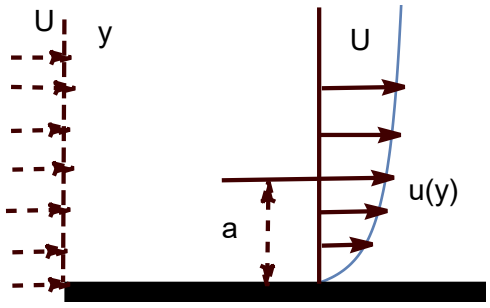

Figure 1: Schematic representation of the physical model.

By introducing the similarity variables

$$u = Uf'(\zeta), \quad v = \sqrt{\frac{\eta U}{2x}}(\zeta f'(\zeta) - f(\zeta)), \quad \zeta = y\sqrt{\frac{U}{2\eta x}}, \tag{5}$$

the chain rule yields

$$\frac{\partial u}{\partial x} = \frac{\partial u}{\partial \zeta}\frac{\partial \zeta}{\partial x} = -\frac{yUf''(\zeta)}{2x}\sqrt{\frac{U}{2\eta x}}, \tag{6}$$

$$\frac{\partial v}{\partial y} = \frac{\partial v}{\partial \zeta}\frac{\partial \zeta}{\partial y} = \frac{yUf''(\zeta)}{2x}\sqrt{\frac{U}{2\eta x}}, \tag{7}$$

$$\frac{\partial u}{\partial y} = \frac{\partial u}{\partial \zeta}\frac{\partial \zeta}{\partial y} = Uf''(\zeta)\sqrt{\frac{U}{2\eta x}}, \tag{8}$$

$$\frac{\partial^2 u}{\partial y^2} = \frac{\partial}{\partial \zeta}\left(\frac{\partial u}{\partial y}\right)\frac{\partial \zeta}{\partial y} = \frac{U^2}{2\eta x}f'''(\zeta). \tag{9}$$

Substituting these into equations (1) and (2) simplifies the latter to

$$f'''(\zeta) + f(\zeta)f''(\zeta) = 0 \tag{10}$$

with the boundary conditions

$$f(0) = \alpha_1, \quad f'(0) = \alpha_2, \quad f'(\infty) = 1. \tag{11}$$

It is crucial to note that the mass transfer parameter α_1 and the velocity parameter α_2 are key factors in determining the nature of the solution. Depending on their values, the system may have no solution, a unique solution, or multiple solutions (specifically, two). This paper will examine these scenarios and identify the critical values of α_1 and α_2. Additionally, when $\alpha_1 > 0$, suction is present, and when $\alpha_2 > 0$, the plate moves downstream from the origin. Furthermore, the wall shear stress is expressed as

$$S = \sqrt{\frac{\rho^3 U^3 \eta}{2x}}f''(0). \tag{12}$$

3 Numerical Methodology

Given the nonlinear nature of the system described by equations (10) and (11), obtaining an exact closed-form solution is challenging and impractical. Therefore, we employ an innovative numerical approach developed by Syam et al. [7, 19], which utilizes the operational matrix method. The following substitutions are made:

$$\lambda_1 = f, \quad \lambda_2 = \lambda_1', \quad \lambda_3 = \lambda_2'. \tag{13}$$

This transforms the original system (10) and (11) into the following set of equations:

$$\lambda_1' = \lambda_2, \quad \lambda_2' = \lambda_3, \quad \lambda_3' = -\lambda_1\lambda_3, \tag{14}$$

$$\lambda_1(0) = \alpha_1, \quad \lambda_2(0) = \alpha_2, \quad \lambda_3(0) = \xi. \tag{15}$$

The parameter ξ is determined by solving the system of equations (14) and (15), followed by the application of the shooting method to meet the boundary condition $\lambda_2(\infty) = 1$.

Given the nonlinear nature of system (14)-(15), obtaining an exact closed-form solution is challenging. Thus, we employ a novel numerical approach based on the operational

matrix technique, as proposed by Syam et al. [7,19]. We represent the system in matrix form as

$$\Lambda' = \Omega(\Lambda(\zeta)), \quad \Lambda(0) = \Lambda_0, \tag{16}$$

where

$$\Lambda = \begin{bmatrix} \lambda_1 \\ \lambda_2 \\ \lambda_3 \end{bmatrix}, \quad \Lambda_0 = \begin{bmatrix} \alpha_1 \\ \alpha_2 \\ \xi \end{bmatrix}, \quad \Omega(\Lambda) = \begin{bmatrix} \lambda_2 \\ \lambda_3 \\ -\lambda_1\lambda_3 \end{bmatrix}. \tag{17}$$

Following the methodology outlined in [7,19], the solution is expressed as

$$\Lambda(\zeta) = \sum_{k=0}^{M} \Lambda_k \varphi_k(\zeta), \tag{18}$$

where $\{\varphi_0(\zeta), \varphi_1(\zeta), \ldots, \varphi_M(\zeta)\}$ represent block pulse functions defined by

$$\varphi_k(\zeta) = \begin{cases} 1, & \text{if } \zeta_k \le \zeta < \zeta_{k+1}, \\ 0, & \text{otherwise,} \end{cases} \tag{19}$$

and $\{\zeta_0, \zeta_1, \ldots, \zeta_{M+1}\}$ denotes a uniform partition of the interval $[0, \zeta_\infty]$ with step size Δ, while $\{\Lambda_0, \Lambda_1, \ldots, \Lambda_M\}$ are constant vectors. Integrating both sides of equation (16) yields

$$\Lambda(\zeta) = \Lambda_0 + \int_0^{\zeta} \Omega(\Lambda(s))\, ds. \tag{20}$$

At $\zeta = \zeta_j$, for $j = 1, 2, \ldots, M+1$, we have

$$\varphi_k(\zeta_j) = \begin{cases} 1, & \text{if } j = k, \\ 0, & \text{otherwise,} \end{cases} \tag{21}$$

which leads to

$$\Lambda(\zeta_j) = \sum_{k=0}^{M} \Lambda_k \varphi_k(\zeta_j) = \Lambda_j. \tag{22}$$

Thus, we can write

$$\begin{aligned} \Lambda(\zeta_j) &= \Lambda_j \\ &= \Lambda_0 + \int_0^{\zeta_j} \Omega(\Lambda(s))\, ds \\ &= \Lambda_0 + \sum_{k=0}^{j-1} \int_{\zeta_k}^{\zeta_{k+1}} \Omega(\Lambda(s))\, ds \\ &= \Lambda_0 + \sum_{k=0}^{j-1} \int_{\zeta_k}^{\zeta_{k+1}} \Omega\left(\sum_{i=0}^{M} \Lambda_i \varphi_i(s)\right) ds. \end{aligned} \tag{23}$$

Since

$$\varphi_k(s) = \begin{cases} 1, & \text{if } i = k, \\ 0, & \text{otherwise,} \end{cases} \qquad s \in [\zeta_k, \zeta_{k+1}), \tag{24}$$

we obtain

$$\Lambda_j = \Lambda_0 + \sum_{k=0}^{j-1} \int_{\zeta_k}^{\zeta_{k+1}} \Omega\left(\Lambda_k\right)\, ds = \Lambda_0 + \Delta \sum_{k=0}^{j-1} \Omega(\Lambda_k).$$

For further details on this approach, including its convergence and error analysis, refer to [7,19]. As indicated in equation (25), this method is direct, iterative, and highly precise for solving nonlinear systems, offering computational efficiency and reduced processing times compared to other methods for similar problems.

4 Validation

To validate the solution, we define the L_2-truncation error as follows:

$$\epsilon(\alpha_1, \alpha_2) = \sqrt{\int_0^1 \parallel \Lambda'(\zeta) - \Omega(\Lambda(\zeta)) \parallel_E^2 \, d\zeta}, \tag{25}$$

where $\parallel \, . \, \parallel_E$ denotes the Euclidean norm. Table 1 presents the computed truncation errors for various values of α_1 and α_2.

α_1	α_2	$\epsilon(\alpha_1, \alpha_2)$
-0.5	0	1.91×10^{-14}
-0.25	0.25	1.94×10^{-14}
0	0.5	11.881×10^{-14}
0.25	0.75	1.80×10^{-14}
0.5	-0.25	1.77×10^{-14}
0.75	-0.5	1.71×10^{-14}

Table 1: The L_2-truncation error for different values of α_1 and α_2.

In Table 2, we evaluate the boundary condition values to compare them with the expected boundary condition $f'(\infty)$ for various values of α_1 and α_2. These values should ideally be 1, indicating that the shooting method used is accurate.

α_1	α_2	$f'(\infty)$
-0.5	0	1.000000000001
-0.25	0.25	1.000000000001
0	0.5	1
0.25	0.75	0.9999999999999
0.5	-0.25	1.000000000001
0.75	-0.5	0.9999999999999

Table 2: The value of $f'(\infty)$.

To compare our results with those in [20], we determine the critical value of the velocity parameter α_{2c}, which dictates whether the system (10)-(11) has a solution for different values of the mass transfer parameter α_1. Our findings align with those reported in Table 3.

α_1	α_{2c}
-0.5	-0.103499999998
-0.25	-0.212499999999
0	-0.354100000001
0.25	-0.52240000001
0.5	-0.720000000000

Table 3: The critical value of the velocity parameter α_{2c}.

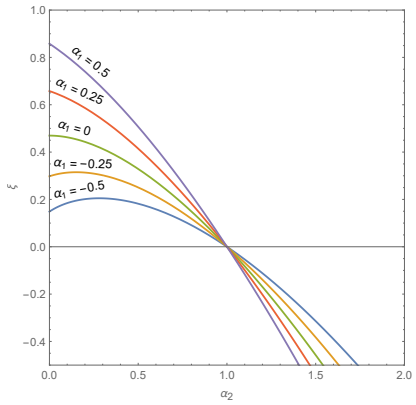

Figure 2: The parametric relationship between the velocity parameter and ξ.

These results suggest that for $\alpha_2 < \alpha_{2c}$, no solution exists. When $\alpha_2 \in [\alpha_{2c}, 0]$, there are two solutions. Finally, for $\alpha_2 > \alpha_{2c}$, a unique solution is obtained. The parametric relationship between α_2 and ξ is shown in Figure 2.

In Figure 3, we investigate the impact of suction and blowing at positive values of the velocity parameter. For $\alpha_2 = 0.5$, the plate moves away from the origin at half the speed of the free stream, whereas for $\alpha_2 = 1.5$, the plate moves approximately 50% faster than the free stream. In both cases, suction increases skin friction, indicated by $f''(0)$, and decreases the boundary layer thickness. Conversely, blowing results in the opposite effect. This phenomenon is depicted in Figure 3.

The results shown in Figure 3 are consistent with the findings of [20]. Additionally, in Figure 4, we explore the effect of the mass transfer parameter α_1 on ξ for different values of the velocity parameter. The outcomes are illustrated in Figure 4.

5 Results and Discussion

The influence of transpiration on self-similar boundary layer flow over moving surfaces was analyzed using the modified operational matrix method. When a uniform stream with velocity U flows parallel to a semi-infinite plate located at $y = 0$ for $x \geq 0$, the flow exhibits no pressure gradient. The velocity components along and perpendicular to the plate are denoted as u and v, respectively. By employing similarity variables, the dimensional unsteady Prandtl boundary layer equations are reduced to a linear boundary value problem of third order. Our numerical method was validated through four approaches: computing the L_2-truncation error, comparing the boundary condition values between

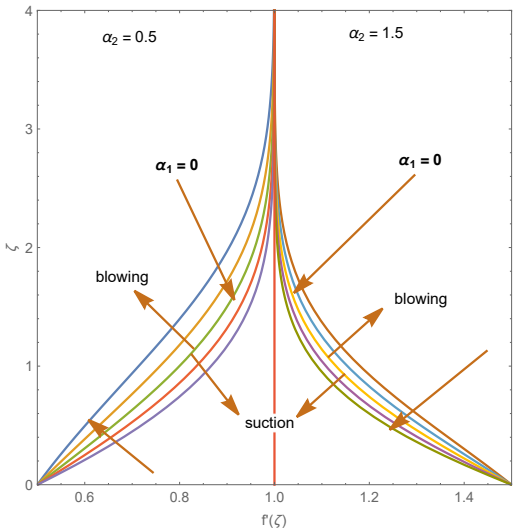

Figure 3: Influence of suction and blowing at positive values of the velocity parameter.

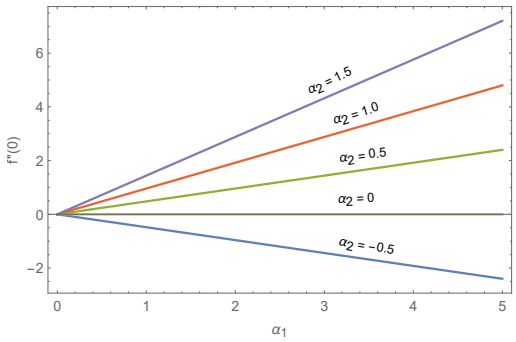

Figure 4: The effect of the mass transfer parameter α_1 on ξ.

the exact condition and those produced by the OMM at ∞, comparing our critical velocity parameter value with that obtained in [20], and graphically comparing our results with those in [20]. These validations are detailed in Tables 1-3 and Figures 2-4.

To gain physical insight into the flow problem and numerical calculations, we graphically discuss the influence of the main parameters in system (10)-(11) in Figures 2 through 16. Figure 2 shows the influence of the velocity parameter on the wall shear stress via $f''(0)$ for different values of the mass transfer parameter α_1. Figure 3 illustrates the effect of suction and blowing at positive values of the velocity parameter. Figure 4 depicts the impact of the mass transfer parameter α_1 on $f''(0)$. Figures 5-8 display the influence of the mass transfer parameter α_1 on the velocity profile when the velocity parameter $\alpha_2 = 0.5, 1.5, 0$ and -0.1. Figures 9-11 examine the effect of the velocity parameter α_2 on the velocity profile for several values of the mass transfer parameter $\alpha_1 = -0.5, 0$ and 0.5. Figures 12-14 analyze the impact of the velocity parameter α_2 on the stream profile for various values of the mass transfer parameter $\alpha_1 = 0, 0.5$, and 1.5. Finally, Figures 15-16 investigate the influence of the mass transfer parameter α_1 on the stream profile when the velocity parameter $\alpha_2 = 0.25$ and 1.25.

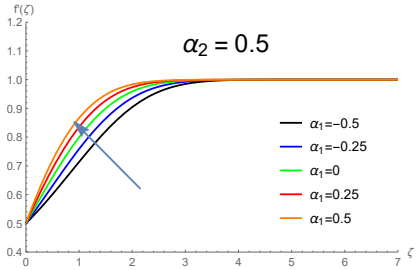

Figure 5: Influence of the mass transfer parameter α_1 on the velocity profile for the velocity parameter $\alpha_2 = 0.5$.

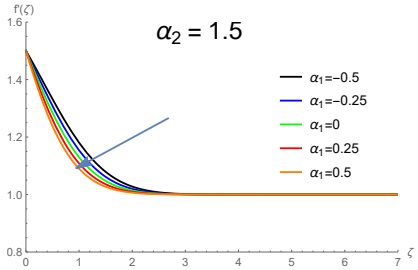

Figure 6: Influence of the mass transfer parameter α_1 on the velocity profile for the velocity parameter $\alpha_2 = 1.5$.

From Figures 2 through 16, we can draw the following conclusions:

1. Table 3 presents the critical values of the velocity parameter. These findings indicate that for $\alpha_2 < \alpha_{2c}$, no solution exists. When $\alpha_2 \in [\alpha_{2c}, 0]$, there are two solutions, and for $\alpha_2 > \alpha_{2c}$, a unique solution is obtained. For instance, when $\alpha_1 = -0.5$, no solution exists for $\alpha_2 < -0.103499999998$, and there are two solutions for $\alpha_2 \in [-0.103499999998, 0]$. For $\alpha_2 > 0$, a unique solution is present.

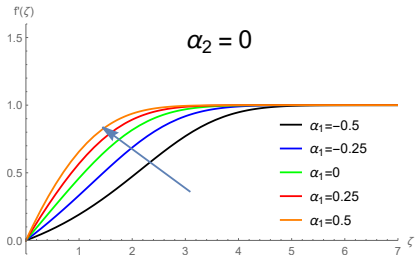

Figure 7: Influence of the mass transfer parameter α_1 on the velocity profile for the velocity parameter $\alpha_2 = 0$.

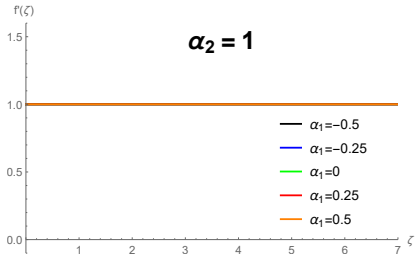

Figure 8: Influence of the mass transfer parameter α_1 on the velocity profile for the velocity parameter $\alpha_2 = 1$.

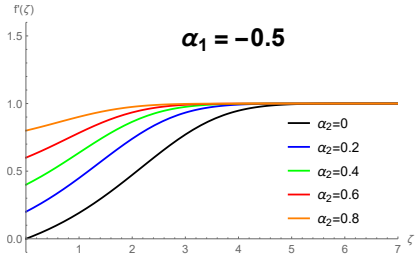

Figure 9: Influence of the velocity parameter α_2 on the velocity profile for the mass transfer parameter $\alpha_1 = -0.5$.

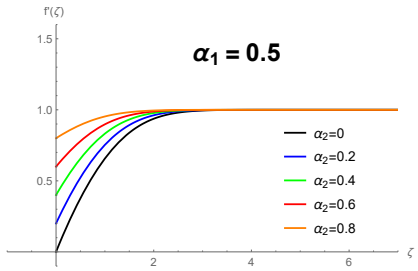

Figure 10: Influence of the velocity parameter α_2 on the velocity profile for the mass transfer parameter $\alpha_1 = 0.5$.

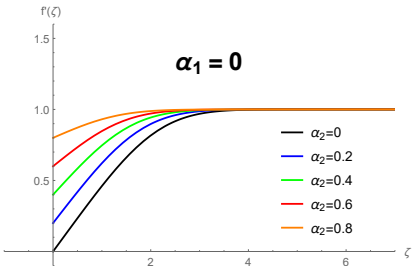

Figure 11: Influence of the velocity parameter α_2 on the velocity profile for the mass transfer parameter $\alpha_1 = 0$.

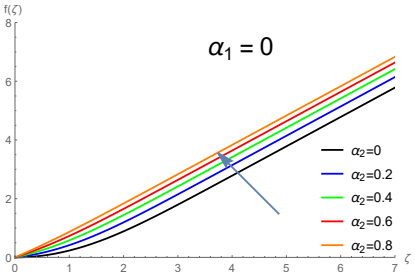

Figure 12: Influence of the velocity parameter α_2 on the stream profile for the mass transfer parameter $\alpha_1 = 0$.

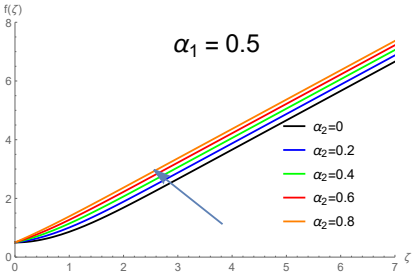

Figure 13: Influence of the velocity parameter α_2 on the stream profile for the mass transfer parameter $\alpha_1 = 0.5$.

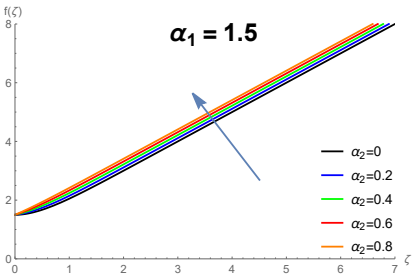

Figure 14: Influence of the velocity parameter α_2 on the stream profile for the mass transfer parameter $\alpha_1 = 1.5$.

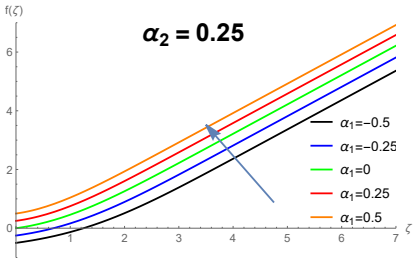

Figure 15: Influence of the mass transfer parameter α_1 on the stream profile for the velocity parameter $\alpha_2 = 0.25$.

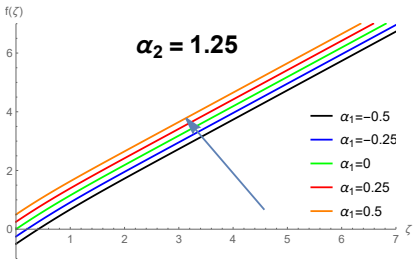

Figure 16: Influence of the mass transfer parameter α_1 on the stream profile for the velocity parameter $\alpha_2 = 1.2$.

The parametric relationship between $\alpha_2 > 0$ and ξ is illustrated in Figure 2. From this figure, it is evident that as the velocity parameter increases for a fixed mass transfer parameter, the wall shear stress decreases.

2. Figure 3 illustrates the impact of suction and blowing at positive values of the velocity parameter. For $\alpha_2 = 0.5$, the plate moves away from the origin at half the speed of the free stream, while for $\alpha_2 = 1.5$, the plate moves approximately 50% faster than the free stream. In both scenarios, suction increases skin friction, as indicated by $f''(0)$, and reduces the boundary layer thickness. Conversely, blowing produces the opposite effect. This phenomenon is depicted in Figure 3. It is also noteworthy that the results shown in Figure 3 are consistent with the findings of [20].

3. Figure 4 explores the effect of the mass transfer parameter $\alpha_1 > 0$ on $\xi = f''(0)$ for different values of the velocity parameter. Additionally, it is observed that as the mass transfer parameter increases for a fixed velocity parameter, the wall shear stress decreases. Furthermore, it is noted that when the velocity parameter is negative, the wall shear stress is in the negative direction, while it is positive when the velocity parameter is positive. It is zero when the velocity parameter is zero.

4. Figures 5-8 demonstrate the effect of the mass transfer parameter α_1 on the velocity profile for different values of the velocity parameter α_2. It is observed that the velocity profiles increase as the mass transfer parameter increases when the velocity parameter is -0.1, 0, and 0.5. The behavior changes when the velocity parameter is

1. From our investigation, we notice that when the velocity parameter is less than one, the velocity profile increases as the mass transfer parameter increases, while the velocity profile decreases as the mass transfer parameter increases when the velocity parameter is greater than one. Notably, when the velocity parameter is one, all velocity profiles coincide for different values of the mass transfer parameter.

5. Figures 9-11 demonstrate the substantial effect of the velocity parameter α_2 on the velocity profile for fixed values of α_1. It is observed that as the velocity parameter increases, the velocity profile also increases. This behavior was examined for various values of the mass transfer parameter such as -0.5, 0, and 0.5. It is noted that the velocity profile stabilizes and approaches one as ξ approaches infinity.

6. Figures 12-14 illustrate the considerable influence of the velocity parameter α_2 on the stream profile for fixed values of α_1. It is observed that as the velocity parameter increases, the stream profile also increases. This behavior was tested for different values of the mass transfer parameter such as 0, 0.5, and 1.5.

7. Figures 15-16 depict the significant impact of the mass transfer parameter α_1 on the stream profile for fixed values of α_2. It is noted that as the mass transfer parameter increases, the stream profile also increases. This behavior was examined for various values of the velocity parameter such as 0.25 and 1.25.

8. Table 1 shows that the L_2-truncation error is of the order 10^{-14}, indicating the rapid convergence of the approximate solution to the exact solution of system (10)-(11).

9. Table 2 reveals that the boundary condition is satisfied, confirming that the shooting method is operating correctly.

Acknowledgment

All authors would like to express their gratitude to the United Arab Emirates University, Al Ain, UAE, for providing financial support with Grant No. 12S116.

References

[1] J.B. Klemp and A.A. Acrivos. A method for integrating the boundary-layer equations through a region of reverse flow. *J. Fluid Mech.* **53** (1972) 177–199.

[2] M.M. Syam and M.I. Syam. Impacts of energy transmission properties on non-Newtonian fluid flow in stratified and non-stratified conditions. *Int. J. Thermofluids* **23** (2024) 100824. https://doi.org/10.1016/j.ijft.2024.100824.

[3] M.Y. Hussaini, W.D. Lakin and N. Nachman. On similarity solutions of a boundary layer problem with an upstream moving wall. *SIAM J. Appl. Math.* **47** (1987) 699–709.

[4] A.-H.I. Mourad, et al. Utilization of additive manufacturing in evaluating the performance of internally defected materials. *IOP Conf. Ser.: Mater. Sci. Eng.* **362** (1) (2018) 012026. https://doi.org/10.1088/1757-899X/362/1/012026.

[5] M.I. Syam, et al. An accurate method for solving the undamped Duffing equation with cubic nonlinearity. *Int. J. Appl. Comput. Math.* **4** (2018) 1–10.

[6] N. Teyar. Properties of MDTM and RDTM for nonlinear two-dimensional Lane-Emden equations. *Nonlinear Dynamics and Systems Theory* **24** (3) (2024) 309–320.

[7] S.M. Syam, Z. Siri, S.H. Altoum, M.A. Aigo and R.M. Kasmani. A new method for solving physical problems with nonlinear phoneme within fractional derivatives with singular kernel. *ASME J. Comput. Nonlinear Dynam.* **19** (2024) 041001. https://doi.org/10.1115/1.4064719.

[8] M.M. Syam, F. Morsi, A. Abu Eida and M.I. Syam. Investigating convective Darcy–Forchheimer flow in Maxwell Nanofluids through a computational study. *Partial Differential Equations in Appl. Math.* **11** (2024) 100863. https://doi.org/10.1016/j.padiff.2024.100863.

[9] M.I. Syam, et al. An accurate method for solving the undamped Duffing equation with cubic nonlinearity. *Int. J. Appl. Comput. Math.* **4** (2) (2018). https://doi.org/10.1007/s40819-018-0502-1.

[10] A. Oultou, O. Baiz and H. Benaissa. Thermo-electroelastic contact problem with temperature dependent friction law. *Nonlinear Dynamics and Systems Theory* **24** (1) (2024) 80–98.

[11] H.M. Jaradat, M. Alquran and M.I. Syam. A reliable study of new nonlinear equation: Two-mode Kuramoto–Sivashinsky. *Int. J. Appl. Comput. Math.* **4** (2018) 64. https://doi.org/10.1007/s40819-018-0497-7.

[12] Salah Al Omari, et al., An investigation on the thermal degradation performance of crude glycerol and date seeds blends using thermogravimetric analysis (TGA), 5th Int. Conf. on Renewable Energy: Generation and Application, ICREGA 2018, 2018-January, pp. 102–106. https://doi.org/10.1109/ICREGA.2018.8337642.

[13] B. Fadlia, A. Zarour, R. Faizi and M. Dalah. Stability analysis of a coupled system of two nonlinear differential equations with boundary conditions. *Nonlinear Dynamics and Systems Theory* **24** (3) (2024) 246–258.

[14] M.I. Syam, M. Sharadga and I. Hashim. A numerical method for solving fractional delay differential equations based on the operational matrix method. *Chaos, Solitons & Fractals* **147** (2021) 110977. https://doi.org/10.1016/j.chaos.2021.110977.

[15] P.D. Weidman, D.G. Kubitschek and A.M.J. Davis. The effect of transpiration on self-similar boundary layer flow over moving surfaces. *Int. J. Eng. Sci.* **44** (2006) 730–737.

[16] L. Abdelhaq, S.M. Syam and M.I. Syam. An efficient numerical method for two-dimensional fractional integro-differential equations with modified Atangana–Baleanu fractional derivative using operational matrix approach. *Partial Differential Equations in Appl. Math.* **11** (2024) 100824. https://doi.org/10.1016/j.padiff.2024.100824.

[17] M.M. Syam, et al. Mini Containers to Improve the Cold Chain Energy Efficiency and Carbon Footprint. *Climate* **10** 76. https://doi.org/10.3390/cli10050076.

[18] T. Syam, et al. *Statistical Analysis of Car Data Using Analysis of Covariance (ANCOVA)*. Springer Proceedings in Mathematics & Statistics, 2023.

[19] S.M. Syam, Z. Siri and R.M. Kasmani. Operational matrix method for solving fractional system of Riccati equations. 2023 International Conference on Fractional Differentiation and Its Applications (ICFDA), Ajman, United Arab Emirates, 2023, pp. 1–6. https://doi.org/10.1109/ICFDA58234.2023.10153350.

[20] P.D. Weidman, D.G. Kubitschek and A.M.J. Davis. The effect of transpiration on self-similar boundary layer flow over moving surfaces. *Int. J. Eng. Sci.* **44** (2006) 730–737. https://doi.org/10.1016/j.ijengsci.2006.04.005.